

Article

Performance and Stability of Metal (Co, Mn, Cu)-Promoted $\text{La}_2\text{O}_2\text{SO}_4$ Oxygen Carrier for Chemical Looping Combustion of Methane

Stefano Cimino , Gabriella Mancino and Luciana Lisi *

Istituto Ricerche sulla Combustione—CNR, 80125 Napoli, Italy; gabiellamancino85@libero.it

* Correspondence: stefano.cimino@cnr.it (S.C.); luciana.lisi@cnr.it (L.L.)

Received: 18 December 2018; Accepted: 23 January 2019; Published: 2 February 2019



Abstract: Oxygen carrier materials based on $\text{La}_2\text{O}_2\text{SO}_4$ and promoted by small amounts (1% wt.) of transition metals, namely Co, Mn and Cu, have been synthesized and characterized by means of X-ray diffraction (XRD), Brunauer–Emmett–Teller (BET), Temperature-programmed reduction/oxidation (TPR/TPO) and thermogravimetry-mass-Fourier transform infrared spectrometry (TG-MS-FTIR) experiments under alternating feeds in order to investigate their potential use for the Chemical Looping Combustion process using either hydrogen or methane as the fuel. The chemical looping reactivity is based on the reversible redox cycle of sulfur from S^{6+} in $\text{La}_2\text{O}_2\text{SO}_4$ to S^{2-} in $\text{La}_2\text{O}_2\text{S}$ and entails a large oxygen storage capacity, but it generally requires high temperatures to proceed, challenging material stability and durability. Herein we demonstrate a remarkable improvement of lattice oxygen availability and activity during the reduction step obtained by cost-effective metal doping in the order $\text{Co} > \text{Mn} > \text{Cu}$. Notably, the addition of Co or Mn has shown a significant beneficial effect to prevent the decomposition of the oxysulfate releasing SO_2 , which is identified as the main cause of progressive deactivation for the unpromoted $\text{La}_2\text{O}_2\text{SO}_4$.

Keywords: oxygen storage capacity; thermal stability; cyclic operation; deactivation; oxysulfate; oxysulfide

1. Introduction

Chemical Looping Combustion (CLC) represents one of the most investigated approaches for clean combustion of fossil fuels because it provides an easy CO_2 capture [1–3] by splitting the process into two cyclic half-steps. The same two-step technology has been also proposed for Chemical Looping Reforming [1–3].

Large oxygen storage capacity (OSC), fast oxidation and reduction kinetics and high stability of the oxygen carrier (OC) are crucial parameters for process development [4]. A large variety of OCs have been proposed, most of them based on transition metals (Cu, Ni, Fe, Mn, Co) as bulk or supported simple oxides or as more complex oxides such as perovskite-like materials [3,5,6]. Perovskites show a better thermal stability and adjustable properties related to the partial or total substitution of A and B metal cations in their ABO_3 structure [6].

Recently, Miccio et al. [7,8] have dispersed iron and iron/manganese oxides into a geopolymer matrix to provide low density materials with good resistance to mechanical stresses that can be suitable for fluidized bed reactors.

Additionally, CaSO_4 has been investigated due to its potentially higher oxygen transport capacity compared to transition metal oxides, deriving from the redox cycle of sulfur [3,9,10]. Nevertheless, a significant sulfur release due to decomposition at high temperature represents an unsolved issue for CaSO_4 , in addition to agglomeration and sintering that are typical of metal oxides (MeOx). An attempt to face the loss of efficiency has been proposed by adding elemental iron [9].

Machida and co-workers [11–16] have deeply investigated rare earths based oxysulfates ($\text{Ln}_2\text{O}_2\text{SO}_4$) as stable, durable, and high performing oxygen storage materials in three ways catalysts for automotive emission control. Sulfur can undergo a complete reduction from S^{6+} in the oxysulfate to S^{2-} in the oxysulfide structure by reaction with a reducing agent and it can be reversibly re-oxidized to S^{6+} by reaction with molecular oxygen, provided that a suitable temperature is chosen for the two processes. Indeed, both the $\text{Ln}_2\text{O}_2\text{SO}_4$ and its corresponding reduced compound $\text{Ln}_2\text{O}_2\text{S}$ crystallize in a similar structure consisting of alternating layers of $\text{Ln}_2\text{O}_2^{2+}$ and SO_4^{2-} or S^{2-} anions. The phase transformation is therefore regarded as the removal or insertion of O^{2-} surrounding sulfur [13]. The thermal stability of $\text{Ln}_2\text{O}_2\text{SO}_4$ decreases with increasing the atomic number of Ln [11,17]. Accordingly, it has been reported that $\text{Lu}_2\text{O}_2\text{SO}_4$ cannot be reduced to the corresponding oxysulfide, since it transforms directly into Lu_2O_3 and SO_2 under reducing atmosphere [16]. Furthermore, Machida et al. [12–14] found that among other Ln-oxysulfates, $\text{Pr}_2\text{O}_2\text{SO}_4$ is able to operate the redox cycles at the lowest temperatures, due to the beneficial effect of the existence of $\text{Pr}^{3+}/\text{Pr}^{4+}$ surface species on the redox of sulfur. They also reported that sulfate reduction becomes easier with increasing distortion of the tetragonal SO_4 unit in the oxysulfate, as evidenced in $\text{Pr}_2\text{O}_2\text{SO}_4$ structure [13]. However, due to the high cost and scarce availability of praseodymium, substitution of the more common lanthanum is difficult to pursue [13]. In conclusion, the oxygen storage properties of $\text{Ln}_2\text{O}_2\text{SO}_4$ can be enhanced (i) by introducing redox species and/or (ii) by increasing distortion of the SO_4 unit as in the case of the partial substitution of Ce for La in $(\text{La}_{1-x}\text{Ce}_x)_2\text{O}_2\text{SO}_4$ [14] and/or (iii) by the addition of noble metals on the surface (1% wt. Pd or Pt), likely promoting the redox cycle of $\text{Ln}_2\text{O}_2\text{SO}_4$ by hydrogen/oxygen spillover effect [11–14].

The cost-effective addition of small quantities of Cu [10] or Na and Fe [18] to $\text{La}_2\text{O}_2\text{SO}_4$, as well as Ni to $\text{Pr}_2\text{O}_2\text{SO}_4$ [19] has been recently reported to enhance oxygen storage capability (OSC) and storage/release reaction rates, in agreement with the distortion of the SO_4 unit [13,15], thus allowing operation at lower temperatures than with parent oxysulfates. It can be argued that cations with different dimensions can alter the lattice to a different extent, thus affecting the OSC and stability of materials.

In this paper, we set out to investigate the effect of the addition of a low amount (1% wt.) of three different transition metals (Cu, Mn, Co) on the OSC as well as on stability/durability of a $\text{La}_2\text{O}_2\text{SO}_4$ oxygen carrier. Chemical looping reaction experiments have been performed under alternating feed conditions at a fixed temperature in the range 700–900 °C, using either hydrogen or methane as the fuel (i.e., reducing agent). The emission of sulfur compounds under repeated redox cycles has been investigated to provide a detailed analysis of conditions promoting the undesired decomposition of the oxygen carrier.

2. Results

In Table 1 the list of metal-promoted OCs is reported with the corresponding values of Brunauer–Emmett–Teller (BET) surface area. The original surface area of the as-prepared $\text{La}_2\text{O}_2\text{SO}_4$ is rather low (2.7 m^2/g), in agreement with previous results reported for the simple preparation method based on the thermal decomposition of bulk lanthanum sulfate at 1027 °C under inert flow [20,21]. The further addition of 1% wt. of transition metals followed by heat treatment at 900 °C does not significantly alter the specific surface area of the materials.

In Figure 1a X-ray diffraction (XRD) patterns of fresh $\text{La}_2\text{O}_2\text{SO}_4$ and transition metal-promoted $\text{La}_2\text{O}_2\text{SO}_4$ are reported. All spectra show the characteristic lines of monoclinic lanthanum oxysulfate (JCPDS 085-1535). The presence of the transition metals causes a decrease of crystallinity, as shown by the lower intensity of XRD peaks, which is particularly evident for the case of Co- $\text{La}_2\text{O}_2\text{SO}_4$. As mentioned in the Introduction, the structure of $\text{La}_2\text{O}_2\text{SO}_4$ consists of alternating stacks of $\text{La}_2\text{O}_2^{2+}$ layers and layers of anions SO_4^{2-} [12,15], therefore the possible inclusion of the transition metal into the lattice can generate a distortion since the radius of the transition metal ion differs from that of La^{3+} (1.03 Å). Notably, for the same oxidation state (including the metallic state), cobalt shows the

smallest dimensions. In particular, the ionic radius of Me^{3+} , supposed to substitute La^{3+} in the lattice, is 0.60 Å for cobalt and 0.70 Å for manganese. Copper, which is generally in the +2 oxidation state, has a ionic radius as Cu^{2+} similar to Mn^{3+} (0.73 Å). That could explain the lowest crystallinity of the $\text{Co-La}_2\text{O}_2\text{SO}_4$ material.

Table 1. List of oxygen carriers and corresponding values of Brunauer–Emmett–Teller (BET) surface area.

Oxygen Carrier	BET Area (m^2/g)
$\text{La}_2\text{O}_2\text{SO}_4$	2.7
$\text{Cu-La}_2\text{O}_2\text{SO}_4$	2.7
$\text{Mn-La}_2\text{O}_2\text{SO}_4$	2.4
$\text{Co-La}_2\text{O}_2\text{SO}_4$	2.4

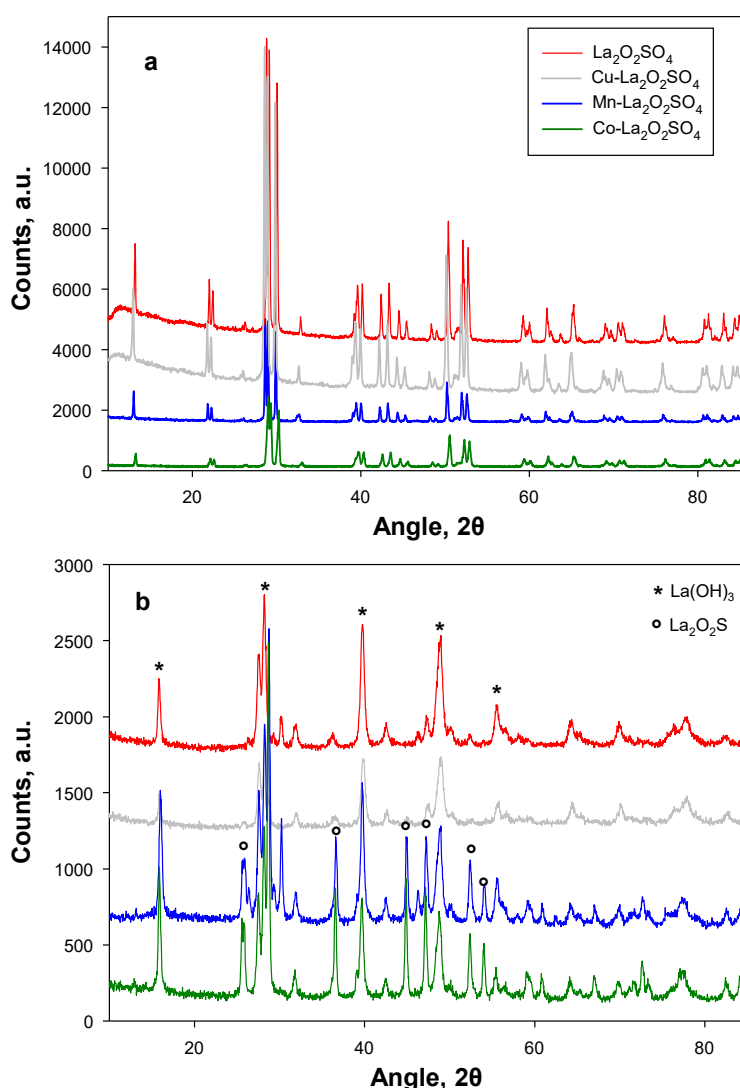


Figure 1. X-ray diffraction (XRD) patterns of (a) as prepared and (b) used (15 cycles at 900°C) $\text{La}_2\text{O}_2\text{SO}_4$ and metal (Cu, Mn, Co) promoted $\text{La}_2\text{O}_2\text{SO}_4$.

The effect of metal doping on the thermal stability of $\text{La}_2\text{O}_2\text{SO}_4$ has been studied by thermogravimetry-mass spectrometry (TG-MS) experiments ramping up to 1300 °C at 10 °C/min under N_2 flow: the corresponding derivative weight loss plots (Figure 2a) are superimposed and flat

for all materials, indicating an almost constant weight up to ca. 1050 °C. Above this temperature, which corresponds well to the decomposition temperature previously reported for La oxysulfate [21], all materials experience a significant weight loss, at similar increasing rates up to 1300 °C, where the process is not yet completed (during 10 min under isothermal conditions). Accordingly, the MS traces for SO₂ ($m/z = 64$), O₂ ($m/z = 32$) and CO₂ ($m/z = 48$) in the evolved gas display similar trends for undoped La₂O₂SO₄ (Figure 2b) as well as for metal-doped materials (exemplified in Figure 2c for the case of Mn-La₂O₂SO₄). In particular, a limited CO₂ release can be observed in the temperature range of 250–500 °C corresponding to the decomposition of some superficial La-carbonates. A rather small SO₂ peak in the range of 800–950 °C suggests the decomposition of some residual La sulfates. Eventually, a large SO₂ release begins at temperatures around 1050 °C, which is accompanied by the evolution of O₂, thus suggesting the occurrence of La oxysulfate decomposition to La₂O₃. Poston et al. [21] detected (by XRD analysis) the simultaneous formation of La₂O₃ and La₂O₂S phases during thermal treatment of La₂O₂SO₄ at $T \geq 1050$ °C in air. According to our results, the oxygen release never occurs independently from SO₂. Therefore, it can be concluded that under N₂ flow none of the doped or undoped La oxysulfates is able to release oxygen and turns spontaneously into the corresponding oxysulfide without decomposing.

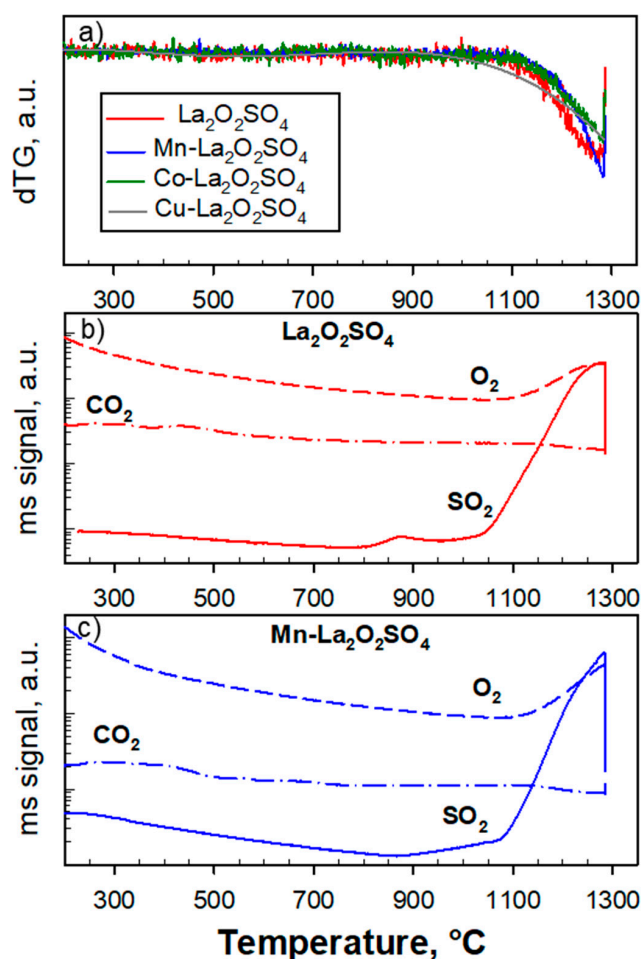


Figure 2. (a) dTG curves for La₂O₂SO₄ and metal (Cu, Mn, Co) promoted La₂O₂SO₄ during heating under a N₂ flow. Heating rate: 10 °C min⁻¹. Corresponding MS temporal profiles for O₂ ($m/z = 32$), CO₂ ($m/z = 44$), and SO₂ ($m/z = 64$) concentration in the evolved gas relevant to (b) La₂O₂SO₄ and (c) Mn-La₂O₂SO₄.

Sequential H₂-TPR/O₂-TPO analysis have been performed to compare the redox behavior of the carriers and results are reported in Figure 3a,b.

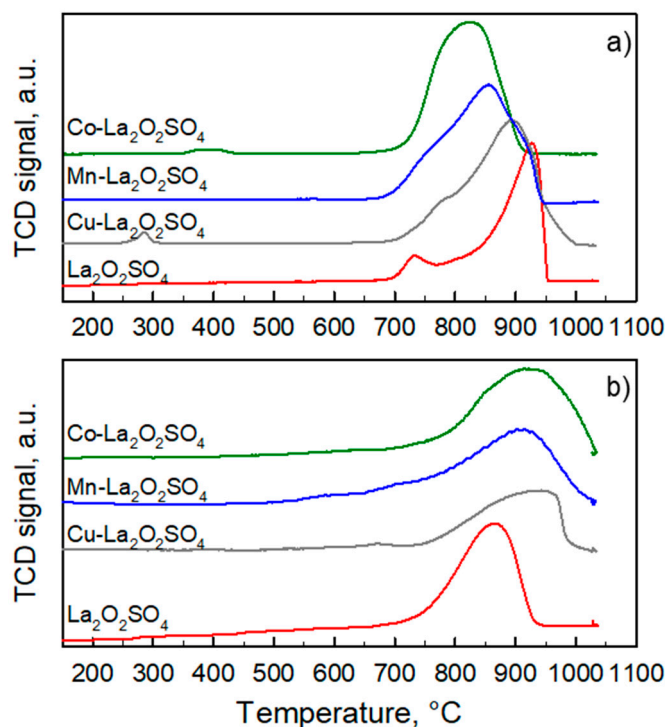


Figure 3. (a) H₂-TPR profiles of La₂O₂SO₄ and metal (Cu, Mn, Co) promoted La₂O₂SO₄; (b) O₂-TPO profiles recorded during the subsequent re-oxidation of OC materials. Heating 10 °C/min from room temperature up to 1030 °C.

The main H₂ consumption event starts for all materials (promoted or not) at ca. 630 °C, and the total H₂ uptake accounts for the complete transformation of La₂O₂SO₄ into the La₂O₂S [10]. However, Co-La₂O₂SO₄ is most easily reduced among others, as testified by the clear shift towards lower temperatures of its H₂ consumption peak showing a maximum at ca. 810 °C. Notably, Cu- and Mn-promoted La₂O₂SO₄ samples show their peaks respectively at 855 °C and 890 °C, whereas the undoped La oxysulfate requires as much as 925 °C. Furthermore, Cu- and Co-promoted OCs display additional small peaks in the low temperature region that can be assigned respectively to the reduction of some segregated/supported CuO and Co₃O₄ [22]. In the case of Mn-La₂O₂SO₄ a very small peak at ca. 560 °C could be related to the reduction of some Mn₂O₃ [23], whereas the eventual presence of Mn₃O₄ could not be detected since its reduction requires higher temperatures [23] and would, therefore, be masked by the onset of reduction of La₂O₂SO₄.

The same trend is confirmed by the results of the TG-MS experiments carried out in the thermo-balance under a 2%H₂/N₂ flow: Figure 4a and Table 2 show all samples experience a similar weight loss (ca. 15.2%), which approaches the theoretical value (15.8%) estimated from the reduction reaction:

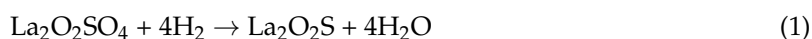


Table 2. Weight loss with onset, inflection, and final temperatures for the reduction of $\text{La}_2\text{O}_2\text{SO}_4$ and metal (Cu, Mn, Co) promoted $\text{La}_2\text{O}_2\text{SO}_4$ under a flow of 2% H_2/N_2 ; amount of SO_2 emitted below 950 °C.

	Δm % wt.	T_{in}	T_{infl} °C	T_{f}	SO_2 Emitted % wt.
$\text{La}_2\text{O}_2\text{SO}_4$	15.2	635	874	972	0.060
Cu- $\text{La}_2\text{O}_2\text{SO}_4$	15.1	625	817	910	0.065
Mn- $\text{La}_2\text{O}_2\text{SO}_4$	15.2	625	784	862	0.009
Co- $\text{La}_2\text{O}_2\text{SO}_4$	15.1	600	690	770	0.009

Small differences are due to some impurities, such as carbonates, which are present in the original samples (Figure 2b,c). In contrast, the complete transformation of $\text{La}_2\text{O}_2\text{SO}_4$ into La_2O_3 would account for a weight loss as large as 19.8%. The onset temperature of weight loss associated with the reduction of $\text{La}_2\text{O}_2\text{SO}_4$ (ca. 630 °C) is not affected by doping with Cu or Mn, whereas Co addition lowers it by 30 °C (Table 2). However, all transition metal (oxides) dopants act as a catalyst to facilitate the surface reaction with the reducing gas, confirming the order of activity is $\text{Cu} < \text{Mn} < \text{Co}$.

In particular, as shown in Table 2, Co-doping lowers the temperature required to complete the transformation of $\text{La}_2\text{O}_2\text{SO}_4$ into $\text{La}_2\text{O}_2\text{S}$ by as much as 200 °C. In the case of Pd- and Pt-promoted $\text{La}_2\text{O}_2\text{SO}_4$ or $\text{Pr}_2\text{O}_2\text{SO}_4$ [11,14] it was inferred that the easier reducibility at lower temperatures is caused by the higher reactivity of atomic hydrogen produced via H_2 spillover from noble metal nanoparticles with respect to molecular H_2 . On the contrary, Me-promoted $\text{La}_2\text{O}_2\text{SO}_4$ materials show similar onset temperatures but, thereafter, reduction proceeds at a significantly faster rate, suggesting this effect could be rather a consequence of distortion of the oxysulfate lattice.

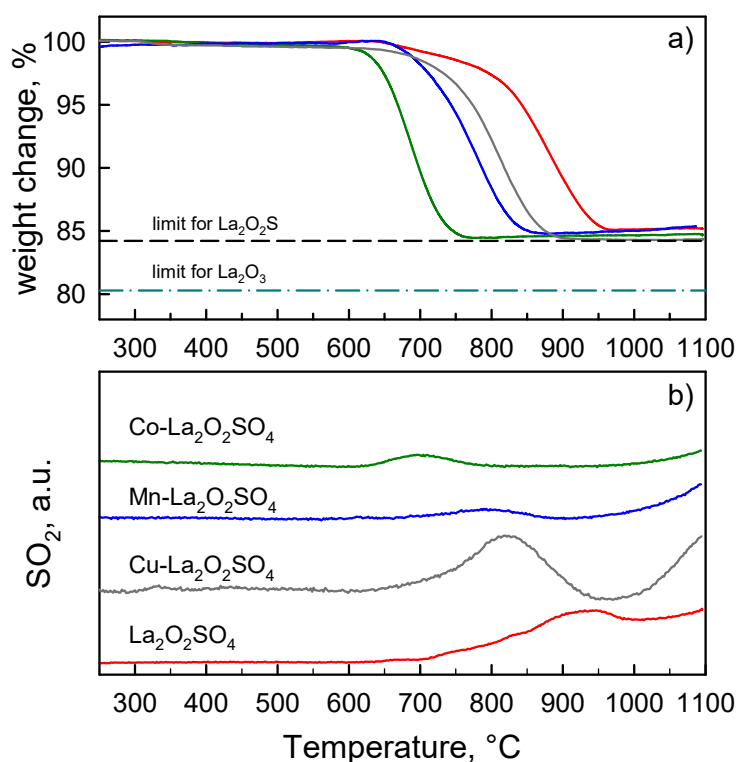
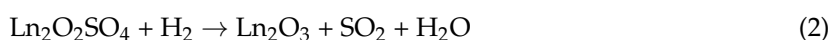


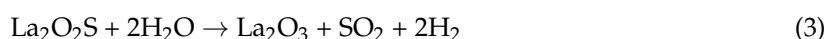
Figure 4. (a) TG curves for $\text{La}_2\text{O}_2\text{SO}_4$ and metal (Cu, Mn, Co) promoted $\text{La}_2\text{O}_2\text{SO}_4$ during reduction under a flow of 2% H_2/N_2 . Heating rate: 10 °C min^{-1} ; (b) Corresponding MS profiles for SO_2 ($m/z = 64$) in the evolved gas.

A serious issue for the durability of La oxysulfates comes from their irreversible decomposition [14] while reacting under a reducing atmosphere. Figure 4b presents the MS profiles for SO₂ emission recorded during TG experiments under H₂/N₂ flow. In fact, besides the H₂ consumption and the corresponding emission of water deriving from its oxidation (not shown), a small SO₂ emission is observed for each material, peaking at the same temperature of the inflection point of the corresponding TG curve (Table 2). Osseni et al. [17] observed by XRD the bulk formation of Lu₂O₃ during Lu₂O₂SO₄ reduction with H₂ at 650, 690 and 800 °C via reaction (2), which possibly occurs to a limited extent also when Ln = La:



In the present case the amount of SO₂ emitted, estimated by peak area after specific calibration, is always rather small: it accounts for ca. 0.06% of the original weight for the case of the undoped and Cu-doped La₂O₂SO₄, whereas it drops down to 0.009% for Co- and Mn-doped materials, possibly due to their faster oxygen mobility and lower temperature level required to complete reduction.

Moreover, a second SO₂ emission starts from 925–945 °C for all OCs. In fact, the two SO₂ emission peaks are partly overlapped for the unpromoted La₂O₂SO₄. It can be argued that the second SO₂ emission corresponds to the decomposition of some residual lanthanum oxysulfate [19]; however, the reaction of La-oxysulfide with residual water [19] present in the chamber cannot be ruled out



Therefore, present results suggest that a faster oxygen mobility in the OC enables operation under conditions far from those leading to a significant and irreversible decomposition.

As shown in Figure 3b, during TPO the undoped La₂O₂S starts to be reoxidized at ca. 700 °C displaying a broad peak centered at 850 °C, with an estimated oxygen consumption corresponding to the theoretical value needed for the restoration of La₂O₂SO₄ [10]. All metal promoted OCs in their oxysulfide form display similar onset temperatures for reoxidation, although the associated O₂ consumption peak is somehow broader than for the undoped material and its maximum occurs at around 900 °C. Unresolved signals also appear in the low-mid temperature region of the TPO profiles of metal-doped OC materials that are related to the reoxidation of Cu or MeOx phases [10].

The oxygen storage performance has been next evaluated at constant temperature under alternating feed stream conditions, where reducing (fuel) and oxidizing (air) gases are cycled. Figure 5 shows the weight changes recorded for doped and undoped OC materials at 800 °C during three cycles obtained alternating 5% H₂/N₂ and air flows. During the first reduction step, all metal-promoted materials undergo a weight loss of ca. 15%, which is compatible with an almost complete reduction of La₂O₂SO₄ to La₂O₂S. However, the unpromoted La₂O₂SO₄ material shows a larger weight loss that slightly exceeds the value expected for the transformation into the corresponding oxysulfide. Moreover, La₂O₂SO₄ needs ca. 40 min to complete its weight loss, whereas all metal promoted samples require a shorter time: the rate of reaction increases in the order Cu < Mn < Co.

Re-oxidation to lanthanum oxysulfate occurs immediately after the exposure to air flow for the three metal promoted materials (showing superimposed TG traces in Figure 5), whilst it takes about 20 min for the unpromoted sample. In fact, the larger weight loss displayed by La₂O₂SO₄ during its first reduction step is irreversible, as confirmed by the incomplete recovery of its original weight after reoxidation. The second and the third cycles show similar qualitative features, Co-La₂O₂SO₄ quickly turning into Co-La₂O₂S and Cu- and Mn-promoted carriers taking few more minutes. On the contrary, the reduction of pure La₂O₂SO₄ appears even harder than in the first cycle, since the weight loss is not completed within the time allowed for this step. Slowing down of the reduction rate of La₂O₂SO₄ after the first reduction/reoxidation cycle was already observed [10] during cyclic H₂-TPR/O₂-TPO experiments with maximum temperatures of 1027 °C. Therefore, a progressive loss of the initial redox properties of La₂O₂SO₄ occurs also when the chemical looping process is operated at a fixed and relatively moderate temperature level.

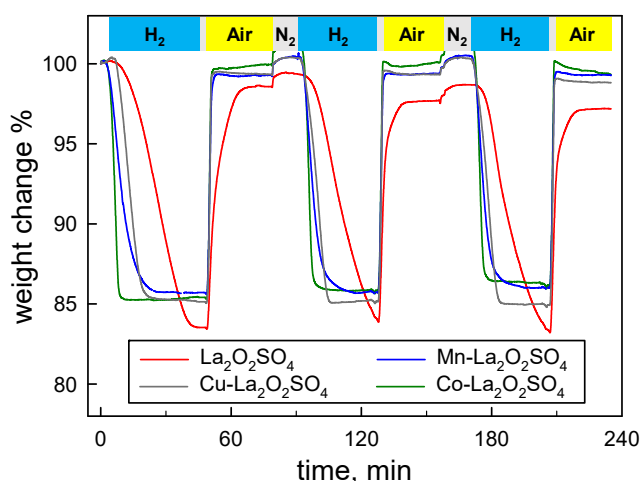


Figure 5. Weight changes during chemical looping reactions under cycled feed stream of 5% CH₄/N₂ and air at 800 °C over La₂O₂SO₄ and metal (Cu, Mn, Co) promoted La₂O₂SO₄.

Lowering the reaction temperature mainly affects the time required to complete the reduction step with H₂, which indeed represents the limiting step, whereas reoxidation in air results always very fast. In fact, due to its intrinsically easier reducibility, only Co-La₂O₂SO₄ is able to complete full redox cycles at 700 °C (not shown) within the given time (45 min).

In order to extend this investigation to a more common fuel, chemical looping combustion in the flow microbalance has been performed using methane (5% vol. in N₂) as the reducing agent. Due to its much lower reactivity with respect to H₂, the operating temperature has been preliminarily set at 900 °C. The oxygen storage performance of the carriers has been verified during 15 cycles (Figure 6), which also allows testing their thermo-chemical stability.

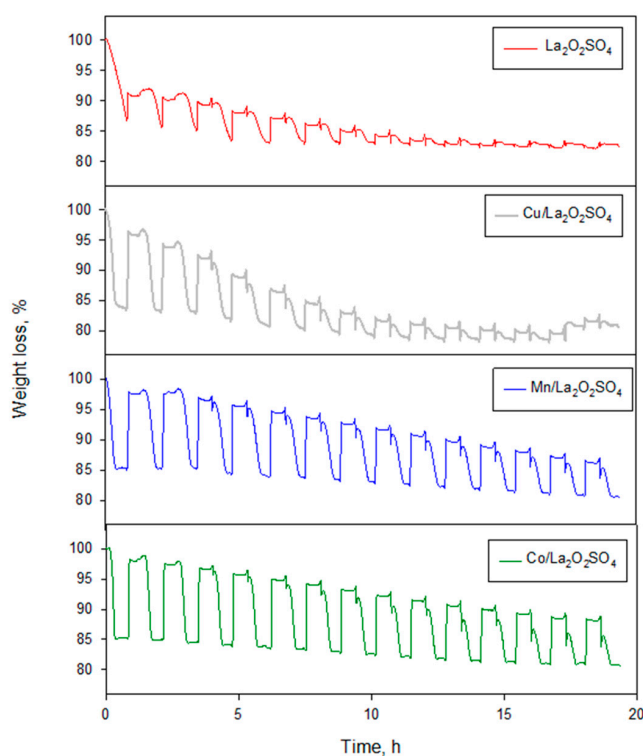
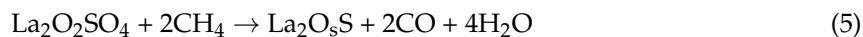
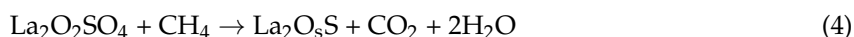


Figure 6. Reducing (under CH₄)/oxidation cycles of La₂O₂SO₄ and metal (Cu, Mn, Co) promoted La₂O₂SO₄ carried out at 900 °C (15 cycles).

All OCs, except the unpromoted one, initially display the typical weight loss of ca. 15%, suggesting the transformation of $\text{La}_2\text{O}_2\text{SO}_4$ into $\text{La}_2\text{O}_2\text{S}$ can occur also by reaction with methane. Judging by the slope of the weight loss profile, the reaction rate increases in the order $\text{Cu} < \text{Mn} < \text{Co}$, thus following the same trend of reactivity found with H_2 as fuel. On the contrary, the weight loss of $\text{La}_2\text{O}_2\text{SO}_4$ is not yet completed after 45 min under CH_4 flow. Thereafter, reoxidation by air does not completely restore the original weight of samples, particularly for those less reactive materials. In fact, the OSC of the undoped $\text{La}_2\text{O}_2\text{SO}_4$ is progressively reduced in the subsequent cycles and vanishes after the 10th cycle.

Doping by copper has a modest beneficial effect on the residual OSC, but the weight of the sample progressively approaches a stable level compatible with the irreversible transformation into La_2O_3 . On the other hand, the promoting effect of manganese and particularly that of cobalt is evident both in terms of reaction rates as well as residual oxygen storage capacity, which is still ca. 45% of its initial value for Co- $\text{La}_2\text{O}_2\text{SO}_4$ during the last cycle.

Figure 7 shows the infrared (IR) spectra of evolved gas collected at three times (initial, middle, end) during the 7th reducing step for Co- $\text{La}_2\text{O}_2\text{SO}_4$. The band around 2340 cm^{-1} is assigned to CO_2 formed by the reaction between CH_4 and lattice oxygen from the material (Equation (4)). CO_2 is the only product detected during the initial phase of reaction over Co- and Mn-doped materials, which promote the deep oxidation of methane with 100% selectivity.



Thereafter, the intensity of the CO_2 signal declines, as a consequence of a reduction in the lattice oxygen mobility/availability and, therefore, in the overall reaction rate. Notably, the appearance of a weak doublet band at $2170\text{--}2115\text{ cm}^{-1}$ (insert of Figure 7) indicates the formation of only small amounts of CO in addition to CO_2 via the partial oxidation of methane (Equation (5)), while the characteristic band centered at 3020 cm^{-1} is associated to increasing amounts of unconverted methane. As expected, a comparison of IR spectra of all OCs (not shown) highlights that the order of deep oxidation rate of methane follows the same trend of lattice oxygen mobility/availability in the OC materials.

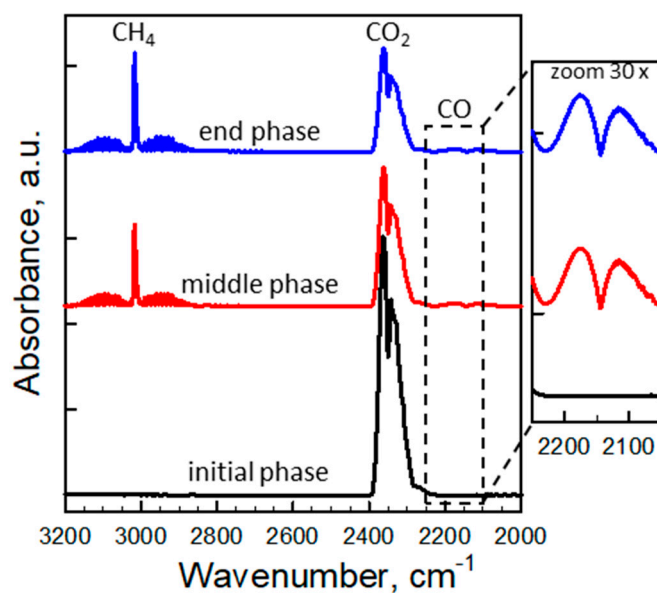
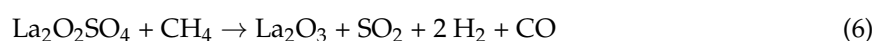


Figure 7. Fourier transform infrared (FTIR) spectra of the evolved gas leaving the TG at three times during the reduction step (under CH_4 flow) of Co- $\text{La}_2\text{O}_2\text{SO}_4$ at $900\text{ }^\circ\text{C}$ (7th cycle of Figure 6). The inset shows a magnification (30x) of the region of typical CO absorption bands.

XRD patterns of $\text{La}_2\text{O}_2\text{SO}_4$ and metal-promoted $\text{La}_2\text{O}_2\text{SO}_4$ at the end of 15 cycles are presented in Figure 1b. The low intensity of signals compared to the corresponding ones in Figure 1a is due to the small amount of each material (12–16 mg) available after the experiments in the flow microbalance. All samples show quite complex patterns suggesting the presence of two or more crystalline phases. In particular they all show a well detectable peak at ca. 13° that can be assigned to lanthanum hydroxide (JCPDS 36–1481) produced by hydration of La_2O_3 . This confirms the loss of oxygen storage capacity is caused by the irreversible decomposition of $\text{La}_2\text{O}_2\text{SO}_4$ with formation of lanthanum oxide. While most of the signals in the XRD patterns of $\text{La}_2\text{O}_2\text{SO}_4$ and $\text{Cu-La}_2\text{O}_2\text{SO}_4$ can be attributed to $\text{La}(\text{OH})_3$, Mn- and Co-promoted carriers still show well detectable peaks at 25° , 28° , 36.9° , 44.9° characteristic of $\text{La}_2\text{O}_2\text{S}_2$ phase. Therefore, the addition of Mn and Co can prevent to some extent the decomposition of lanthanum oxysulfate/oxysulfide. This represents an interesting result considering that the enhancement of oxygen mobility is probably associated with a higher distortion of SO_4 units caused by inclusion of cobalt or manganese ions into the oxysulfate/oxysulfide structure. Therefore, the better crystallized, un-promoted $\text{La}_2\text{O}_2\text{SO}_4$ is more prone to loose sulfate units than the more amorphous $\text{Co-La}_2\text{O}_2\text{SO}_4$.

In order to get further insights into the possible reactions occurring during cycled anaerobic oxidation of methane over the best performing $\text{Co-La}_2\text{O}_2\text{SO}_4$, further TG experiments have been carried out analyzing evolved gases with the mass spectrometer. Figure 8 shows the weight change and the corresponding mass signals for the main gaseous products ($m/z = 2, 18, 44, 64$) as recorded at 900°C by alternating reducing and oxidizing flows (40min), separated by a N_2 purge (30 min) in between. As soon as exposed to methane, $\text{Co-La}_2\text{O}_2\text{SO}_4$ is quickly and completely reduced according to equation (4), giving H_2O and CO_2 as primary products, as confirmed by the sharp and simultaneous MS peaks recorded in the effluent gas. After the expected weight loss (ca. 15.5%) is completed, a small weight increase is observed, that is probably related to some coke deposition on the sample deriving from CH_4 decomposition catalyzed by Co [24]. Accordingly, a sudden emission of H_2 shows up after the production of CO_2 and water has stopped, and it continues during the purge phase, as long as some methane is still available in the reacting chamber. While the lattice oxygen from the OC material is consumed to oxidize methane, an evident peak of SO_2 emission appears that ends when the OC is fully reduced. Notably, the maximum SO_2 concentration is ca. two orders of magnitude lower than CO_2 . This phenomenon resembles what observed during H_2 -TPR experiments (Figure 4), and indicates a limited decomposition of $\text{La}_2\text{O}_2\text{SO}_4$ can occur also by reaction with methane leading to SO_2 and the products of methane partial oxidation (Equation (6)):



However, the formation of CO ($m/z = 28$) cannot be easily detected because of the use of N_2 as the carrier gas.

Due to the formation of some La_2O_3 , the OC material cannot fully recover its original weight during the fast oxidation occurring as soon as it is exposed to air flow. During this phase, a small CO_2 peak appears, caused by the oxidation of coke deposits previously formed on the material. The stepwise increase in the signal of H_2O is assigned to humidity contained in the air flow. Moreover, a new but rather small emission of SO_2 is detected during the reoxidation, therefore the occurrence of reaction (7) should be also considered:



During the subsequent cycles, the temporal profiles of the gaseous species are repeatable.

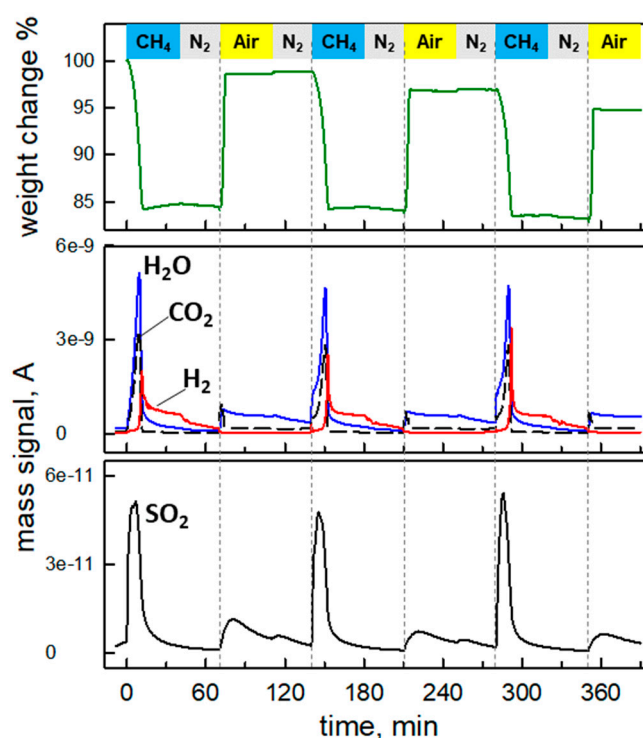


Figure 8. Weight change and gas concentration profiles during chemical looping reactions under cycled feed stream of 5% CH₄/N₂ and air at 900 °C over Co-La₂O₂SO₄.

Considering the high oxygen mobility in Co-La₂O₂SO₄, the cyclic anaerobic oxidation of methane has been tested also at 800 °C and 750 °C in order to verify if the adverse impact of decomposition reactions (Equations (6) and (7)) could be limited. Results are shown in Figures 9 and 10, respectively. As expected, at 800 °C the reduction of the oxysulfate takes place at a slower rate but the corresponding weight loss is completed within ca. 30 min under CH₄ flow. Accordingly, water and CO₂ are produced during the whole reduction phase, resulting in wider emission peaks than at 900 °C. Some H₂ appears only at the end of this step, but is not accompanied by any detectable weight increase. It is inferred that CH₄ decomposition does not significantly proceed at 800 °C, whereas some methane partial oxidation can occur when lattice oxygen from the OC is almost completely exploited. The SO₂ emission during the reduction step at 800 °C is at least one order of magnitude lower than at 900 °C, confirming the hypothesis on the beneficial effect of a lower reaction temperature to limit the decomposition of the oxysulfate into the corresponding oxide. Re-oxidation under air at 800 °C is still very rapid, and the weight recovery is almost complete. However, the second (and third) reduction step is slower than the first one so that the transformation into the oxysulfide phase ends only during the purging step. As a consequence, CO₂ and H₂O profiles show broader peaks with similar area but lower maxima with respect to the first cycle and shifted towards the end of the period. The SO₂ emission during reoxidation remains quite low. The results of the third cycle are repeatable.

As shown on the top of Figure 10, when operating at 750 °C the duration of the reduction step has been prolonged up to 90 min. The slower rate of reduction of the OC material limits its final weight loss to 15.3%, indicating that the transformation into the oxysulfide phase is not yet completed and ca. 96.5% of the total OSC has been consumed. The corresponding production of water and CO₂ by methane oxidation with lattice oxygen is characterized by the presence of two emission peaks: the first one is sharp and located at the beginning of the exposure to CH₄, whereas the second peak is broad and centered at ca. 45 min. It can be argued that the initial formation of an outer shell of La₂O₂S may slow down the reaction due to the increase of diffusional limitations (in the solid state). H₂ formation is initially low and increases towards the end of the period, testifying an increase of process selectivity towards the products of partial oxidation of methane due to the slow oxygen availability from the

OC material. However, no SO_2 emission can be detected (sub-ppm level) during operation at $750\text{ }^\circ\text{C}$. The subsequent reoxidation by air is still fast. As already observed at $800\text{ }^\circ\text{C}$, the second reduction step is slower than the first one: based on the final weight of the OC, ca. 80% of its total OSC has been utilized. Moreover, the fraction of $\text{La}_2\text{O}_2\text{S}$ displays a lower attitude to be fully re-oxidized, since the sample does not completely recover its previous weight. The results of the third cycle are repeatable, confirming that the partial reduction of the OS performance is not related to material stability issues (decomposition) but rather to an incomplete transformation between $\text{La}_2\text{O}_2\text{SO}_4$ and $\text{La}_2\text{O}_2\text{S}$ phases due to the reduced oxygen mobility.

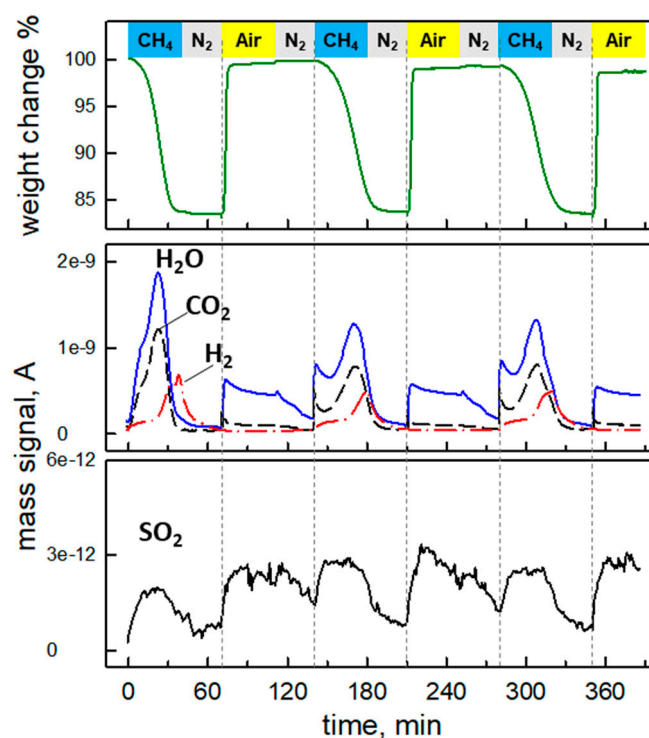


Figure 9. Weight change and gas concentration profiles during chemical looping reactions under cycled feed stream of 5% CH_4/N_2 and air at $800\text{ }^\circ\text{C}$ over $\text{Co-La}_2\text{O}_2\text{SO}_4$.

Overall the results indicate that the Co-promoted $\text{La}_2\text{O}_2\text{SO}_4/\text{La}_2\text{O}_2\text{S}$ couple can be favorably operated at $800\text{ }^\circ\text{C}$ in the chemical looping combustion of methane: it shows a high oxygen mobility that promotes complete oxidation of methane and full exploitation of its outstanding OS capacity, and a remarkable stability/durability during cyclic operation. Notably, the stability of the $\text{La}_2\text{O}_2\text{SO}_4/\text{La}_2\text{O}_2\text{S}$ system could be strongly enhanced in the presence of even small contents of S-bearing compounds [14], commonly found in the fuel stream. On the other hand, further studies should address the possibility to enhance lattice oxygen mobility and overall reactivity at lower temperatures, by increasing the specific surface area of the OC [18], and by varying the content of transition metal (oxide) dopant which could effectively work as an intermediate oxygen gateway [16] apart from its role as structural promoter.

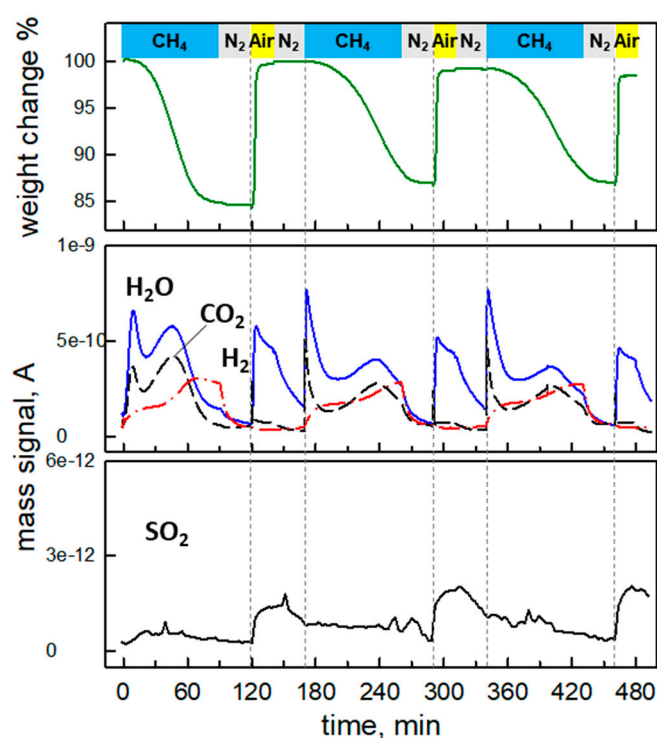


Figure 10. Weight change and gas concentration profiles during chemical looping reactions under cycled feed stream of 5% CH₄/N₂ and air at 750 °C over Co-La₂O₂SO₄.

3. Materials and Methods

3.1. Preparation of Oxygen Carriers

Lanthanum oxysulfate (La₂O₂SO₄) was obtained starting from La₂(SO₄)₃ (Sigma-Aldrich, 99.99% purity, St. Louis, MO, USA) by heating it at 1027 °C for 5 h under helium flow [10,20]. Different fractions of La₂O₂SO₄ powder were impregnated with water solutions of Cu(NO₃)₂·2.5H₂O (Sigma-Aldrich, purity ≥ 98%, St. Louis, MO, USA), Mn(NO₃)₂·4H₂O (Sigma-Aldrich, purity ≥ 97%, St. Louis, MO, USA) and Co(NO₃)₂·6H₂O (Sigma-Aldrich, purity ≥ 98%, St. Louis, MO, USA) to obtain samples with a nominal 1wt% metal loading. After impregnation, samples were dried for 12 h at 120 °C in a stove and eventually heat treated at 900 °C for 2 h under He.

3.2. Physical and Chemical Characterization

The surface area was evaluated according to the BET method by N₂ adsorption at 77K with a Quantachrome Autosorb 1-C analyzer (Quantachrome Instruments, Boynton Beach, FL, USA).

Powder X-ray diffraction (XRD) analysis was performed with a Bruker D2 Phaser diffractometer (Bruker, Billerica, MA, USA) operated at diffraction angles ranging between 10 and 80° 2θ with a scan rate of 0.02° 2θ s⁻¹.

Temperature Programmed Reduction (TPR) and Oxidation (TPO) experiments were carried out with a Micromeritics Autochem II TPD/TPR instrument (Micromeritics, Norcross, GA, USA) equipped with a TC detector. The samples (20–30 mg) were first reduced under a flow of 2% H₂ in Ar (50 Ncm³/min) by heating up to 1027 °C at 10 °C/min; thereafter, they were reoxidized under a flow of 0.5% O₂ in He (50 Ncm³/min) using the same temperature ramp.

TG analysis were performed in a Setaram Labsys Evo TGA-DTA-DSC 1600 (Setaram Instrumentation, Caluire, France) flow microbalance loading 15–25 mg of sample in an alumina crucible and ramping the temperature at 10 °C/min up to 1300 °C or 1150 °C, respectively under a flow (100 cc/min) of pure N₂ or 2% H₂ in N₂.

3.3. Chemical Looping Reaction

Cyclic isothermal reduction/oxidation tests were carried out in the same Setaram Labsys Evo flow microbalance at 700, 750, 800 and 900 °C, by switching alternatively the flow between 5% H₂ (or CH₄) in N₂ and air, at a fixed total flow rate of 100 cc/min. If not otherwise stated, the duration of the reduction phase was 45 min, whilst that of oxidation phase was 30 min, with an intermediate purge by pure N₂ (2–30 min). The evolved gases, leaving the flow microbalance through two independent heated capillaries, were analyzed by a Pfeiffer ThermoStar G mass spectrometer and a Perkin Elmer Spectrum GX spectrometer in order to detect all IR-active gaseous species. In this last case, IR spectra were rationed against a background spectrum of pure N₂ and were collected every 1–10 min depending on the duration of the experiment.

4. Conclusions

Oxygen carrier materials based on La₂O₂SO₄ promoted by small amounts (1% wt.) of transition metals such as Co, Mn and Cu have been synthesized and characterized by means of XRD, BET, TPR/TPO and TG-MS-FTIR experiments in order to investigate their potential use in the Chemical Looping Combustion process with either hydrogen or methane as fuel. Results demonstrate that doping the parent La₂O₂SO₄ with transition metals can promote lattice oxygen mobility in the temperature range 700–900 °C following the order Cu < Mn < Co, catalyzing the complete reduction of La₂O₂SO₄ to form La₂O₂S by reaction with either H₂ and CH₄. On the other hand, the reoxidation of La₂O₂S by molecular oxygen to restore the La₂O₂SO₄ phase requires temperatures ≥700 °C to proceed quickly and is poorly affected by the addition of those transition metals.

Notably, the addition of Co or Mn has shown a marked beneficial effect to limit or inhibit the decomposition of the oxysulfate that releases some SO₂. Such undesired side reaction proceeds to some extent together with the main reduction of the La₂O₂SO₄ by either H₂ or CH₄ and it causes a progressive and irreversible loss of the original oxygen storage capacity through the formation of the stable La₂O₃ phase. Eventually, metal doping does not affect the thermal decomposition of La₂O₂SO₄ occurring above ca. 1030 °C under inert flow, nor it promotes any spontaneous reduction of the lanthanum oxysulfate to oxysulfide.

The enhanced performance of the Co-promoted carrier can be assigned to H₂/CH₄ activation on metal sites and to the higher distortion of SO₄ units in the oxysulfate lattice caused by the partial inclusion of Co³⁺ ion, much smaller than La³⁺, which enhances oxygen mobility.

TG-MS-FTIR experiments of CLC with alternating feeds have shown that Co-La₂O₂SO₄ is able to oxidize CH₄ at 800 °C producing CO₂ and water with reasonable rates and high selectivity, avoiding the deterioration of performance related to a progressive decomposition. At higher temperatures, the oxygen storage performance is progressively lost due to the irreversible formation of some La₂O₃, that occurs as a side reaction during the reducing step of the OC material by the fuel and is accompanied by the release of SO₂. At lower temperatures, the mobility of lattice oxygen becomes the limiting factor that can preclude the complete exploitation of the OSC within a reasonable contact time with the fuel stream.

Author Contributions: Data curation, G.M.; Investigation, S.C., G.M. and L.L.; Supervision, S.C. and L.L.; Writing—original draft, S.C. and L.L.; Writing—review & editing, S.C.

Funding: This research received no external funding.

Acknowledgments: Luciano Cortese is kindly acknowledged for XRD analysis.

Conflicts of Interest: The authors declare no conflict of interest.

References

1. Tang, M.; Xu, L.; Fan, M. Progress in oxygen carrier development of methane-based chemical-looping reforming: A review. *Appl. Energy* **2015**, *151*, 143–156. [[CrossRef](#)]

2. Bhavsar, S.; Najera, M.; Solunke, R.; Vesper, G. Chemical looping: To combustion and beyond. *Catal. Today* **2014**, *228*, 96–105. [[CrossRef](#)]
3. Adanez, J.; Abad, A.; Garcia-Labiano, F.; Gayan, P.; de Diego, L.F. Progress in Chemical-Looping Combustion and Reforming technologies. *Prog. Energy Combust. Sci.* **2012**, *38*, 215–282. [[CrossRef](#)]
4. Zheng, X.; Che, L.; Hao, Y.; Su, Q. Cycle performance of Cu-based oxygen carrier based on a chemical-looping combustion process. *J. Energy Chem.* **2016**, *25*, 101–109. [[CrossRef](#)]
5. Imanieh, M.H.; Rad, M.H.; Nadarajah, A.; González-Platas, J.; Rivera-López, F.; Martín, I.R. Novel perovskite ceramics for chemical looping combustion application. *J. CO₂ Util.* **2016**, *13*, 95–104. [[CrossRef](#)]
6. Liu, L.; Taylor, D.D.; Rodriguez, E.E.; Zachariah, M.R. Influence of transition metal electronegativity on the oxygen storage capacity of perovskite oxides. *Chem. Commun.* **2016**, *52*, 10369–10372. [[CrossRef](#)] [[PubMed](#)]
7. Miccio, F.; Bendoni, R.; Piancastelli, A.; Medri, V.; Landi, E. Geopolymer composites for chemical looping combustion. *Fuel* **2018**, *225*, 436–442. [[CrossRef](#)]
8. Bendoni, R.; Miccio, F.; Medri, V.; Landi, E. Chemical looping combustion using geopolymer-based oxygen carriers. *Chem. Eng. J.* **2018**, *341*, 187–197. [[CrossRef](#)]
9. Bi, W.; Chen, T.; Zhao, R.; Wang, Z.; Wu, J.; Wu, J. Characteristics of a CaSO₄ oxygen carrier for chemical-looping combustion: Reaction with polyvinylchloride pyrolysis gases in a two-stage reactor. *RSC Adv.* **2015**, *5*, 34913–34920. [[CrossRef](#)]
10. Lisi, L.; Mancino, G.; Cimino, S. Chemical looping oxygen transfer properties of Cu-doped lanthanum oxysulfate. *Int. J. Hydrogen Energy* **2015**, *40*, 2047–2054. [[CrossRef](#)]
11. Machida, M.; Kawamura, K.; Ito, K. Novel oxygen storage mechanism based on redox of sulfur in lanthanum oxysulfate/oxysulfide. *Chem. Commun. (Camb.)* **2004**, *2*, 662–663. [[CrossRef](#)] [[PubMed](#)]
12. Machida, M.; Kawamura, K.; Ito, K.; Ikeue, K. Large-Capacity Oxygen Storage by Lanthanide Oxysulfate/Oxysulfide Systems. *Chem. Mater.* **2005**, *17*, 1487–1492. [[CrossRef](#)]
13. Machida, M.; Kawano, T.; Eto, M.; Zhang, D.; Ikeue, K. Ln Dependence of the Large-Capacity Oxygen Storage/Release Property of Ln Oxysulfate/Oxysulfide Systems. *Chem. Mater.* **2007**, *19*, 954–960. [[CrossRef](#)]
14. Ikeue, K.; Eto, M.; Zhang, D.J.; Kawano, T.; Machida, M. Large-capacity oxygen storage of Pd-loaded Pr₂O₂SO₄ applied to anaerobic catalytic CO oxidation. *J. Catal.* **2007**, *248*, 46–52. [[CrossRef](#)]
15. Zhang, D.; Yoshioka, F.; Ikeue, K.; Machida, M. Synthesis and Oxygen Release/Storage Properties of Ce-Substituted La-Oxysulfates, (La_{1-x}Ce_x)₂O₂SO₄. *Chem. Mater.* **2008**, *20*, 6697–6703. [[CrossRef](#)]
16. Zhang, D.; Kawada, T.; Yoshioka, F.; Machida, M. Oxygen Gateway Effect of CeO₂/La₂O₂SO₄ Composite Oxygen Storage Materials. *ACS Omega* **2016**, *1*, 789–798. [[CrossRef](#)]
17. Osseni, S.A.; Denisenko, Y.G.; Fatombi, J.K.; Sal'nikova, E.I.; Andreev, O.V. Synthesis and characterization of Ln₂O₂SO₄ (Ln = Gd, Ho, Dy and Lu) nanoparticles obtained by coprecipitation method and study of their reduction reaction under H₂ flow. *J. Nanostruct. Chem.* **2017**, *7*, 337–343. [[CrossRef](#)]
18. Zhang, W.; Arends, I.W.C.E.; Djanashvili, K. Nanoparticles of lanthanide oxysulfate/oxysulfide for improved oxygen storage/release. *Dalt. Trans.* **2016**, *45*, 14019–14022. [[CrossRef](#)]
19. Tan, S.; Li, D. Enhancing Oxygen Storage Capability and Catalytic Activity of Lanthanum Oxysulfide (La₂O₂S) Nanocatalysts by Sodium and Iron/Sodium Doping. *ChemCatChem* **2018**, *10*, 550–558. [[CrossRef](#)]
20. Sal'nikova, E.I.; Kaliev, D.I.; Andreev, P.O. Kinetics of phase formation upon the treatment of La₂(SO₄)₃ and La₂O₂SO₄ in a hydrogen flow. *Russ. J. Phys. Chem. A* **2011**, *85*, 2121–2125. [[CrossRef](#)]
21. Poston, J.A.; Siriwardane, R.V.; Fisher, E.P.; Miltz, A.L. Thermal decomposition of the rare earth sulfates of cerium(III), cerium(IV), lanthanum(III) and samarium(III). *Appl. Surf. Sci.* **2003**, *214*, 83–102. [[CrossRef](#)]
22. Arnone, S.; Bagnasco, G.; Busca, G.; Lisi, L.; Russo, G.; Turco, M. Catalytic combustion of methane over transition metal oxides. *Stud. Surf. Sci. Catal.* **1998**, *119*, 65–70.
23. Cimino, S.; Lisi, L.; Tortorelli, M. Low temperature SCR on supported MnOx catalysts for marine exhaust gas cleaning: Effect of KCl poisoning. *Chem. Eng. J.* **2016**, *283*, 223–230. [[CrossRef](#)]
24. Zhang, Y.; Smith, K.J. CH₄ decomposition on Co catalysts: Effect of temperature, dispersion, and the presence of H₂ or CO in the feed. *Catal. Today* **2002**, *77*, 257–268. [[CrossRef](#)]

